

New limits on “odderon” amplitudes from analyticity constraints

Martin M. Block

*Department of Physics and Astronomy,
Northwestern University, Evanston, IL 60208*

Kyungsik Kang

*Department of Physics,
Brown University, Providence, RI, 02912*

Abstract

In studies of high energy pp and $\bar{p}p$ scattering, the odd (under crossing) forward scattering amplitude accounts for the difference between the pp and $\bar{p}p$ cross sections. Typically, it is taken as $f_- = -\frac{p}{4\pi} D s^{\alpha-1} e^{i\pi(1-\alpha)/2}$ ($\alpha \sim 0.5$), which has $\Delta\sigma, \Delta\rho \rightarrow 0$ as $s \rightarrow \infty$, where ρ is the ratio of the real to the imaginary portion of the forward scattering amplitude. However, the odd-signatured amplitude can have in principle a strikingly different behavior, ranging from having $\Delta\sigma \rightarrow$ non-zero constant to having $\Delta\sigma \rightarrow \ln s/s_0$ as $s \rightarrow \infty$, the maximal behavior allowed by analyticity and the Froissart bound. We reanalyze high energy pp and $\bar{p}p$ scattering data, using new analyticity constraints, in order to put new and precise limits on the magnitude of “odderon” amplitudes.

The conventional odd (under crossing) laboratory forward scattering amplitude used for pp and $\bar{p}p$ scattering, suggested by Regge theory, is

$$\frac{4\pi}{p}f_- = -Ds^{\alpha-1}e^{i\pi(1-\alpha)/2}, \quad (1)$$

which results in $\Delta\sigma \equiv \sigma_{pp} - \sigma_{\bar{p}p} \rightarrow 0$, $\Delta\rho \equiv \rho_{pp} - \rho_{\bar{p}p} \rightarrow 0$ as $s \rightarrow \infty$. Nicolescu et al[1, 2, 3] have introduced odd amplitudes called “odderons”, with the interesting properties that they can have $\Delta\sigma \rightarrow$ non-zero constant to even having $\Delta\sigma \rightarrow \ln s/s_0$ as $s \rightarrow \infty$.

There has been mounting evidence from many sources that the crossing-even hadron-hadron cross section behaves at high energy as $\ln^2 s$, thus saturating the Froissart bound, a result with a rather profound physical significance. Using factorization and *simultaneously* fitting real analytic forward scattering amplitudes to $\gamma\gamma$ cross sections, γp cross sections and pp and $\bar{p}p$ cross sections and ρ -values, Block and Kang[4] have shown that a $\ln^2 s$ fit, saturating the Froissart bound, is in accord with the experimental data. The COMPETE group[5], globally fitting hadron-hadron cross sections, has offered evidence that favors a $\ln^2 s$ behavior at high energies. Igi and Ishida[6, 7] have shown that the $\pi^\pm p$ systems and the pp and $\bar{p}p$ systems saturate the Froissart bound, using finite energy sum rules. Kang and Nastase[8] proved that saturation of the QCD Froissart bound is related to the creation of black holes of AdS size in Planckian scattering. Block and Halzen have shown that the Froissart bound is saturated for the γp system[9], the $\pi^\pm p$ systems and the pp and $\bar{p}p$ systems[10], i.e., the even (under crossing) cross section rose asymptotically as $\ln^2 s$. For their nucleon-nucleon analysis they used 4 analyticity constraints that anchored the high energy cross section parametrizations to both the experimental pp and $\bar{p}p$ cross sections and their first derivatives at $\sqrt{s} = 4$ GeV, giving fits with the smallest statistical parameter errors. This technique completely ruled out the possibility of an asymptotic $\ln s$ rise. In this communication we extend their analysis to include “odderons”.

Block and Cahn[11] made an odderon analysis of pp and $\bar{p}p$ scattering in 1985 that put limits on odderon amplitudes. Since we will later want to directly compare our results with theirs, we will use their notation. Using forward real analytic amplitudes to describe the data, they wrote[11] the crossing-even real analytic laboratory amplitude for forward high energy scattering as

$$\frac{4\pi}{p}f_+ = i \left\{ A + \beta[\ln(s/s_0) - i\pi/2]^2 + cs^{\mu-1}e^{i\pi(1-\mu)/2} - i\frac{4\pi}{p}f_+(0) \right\}, \quad (2)$$

and the conventional crossing-odd real analytic forward amplitude as

$$\frac{4\pi}{p}f_- = -Ds^{\alpha-1}e^{i\pi(1-\alpha)/2}. \quad (3)$$

Here $\alpha < 1$ parametrizes the Regge behavior of the crossing-odd amplitude which vanishes at high energies and A , α , β , c , D , s_0 and μ are real constants. The variable s is the square of the center of mass system (c.m.) energy, p is the laboratory momentum. The additional real constant $f_+(0)$ is the subtraction constant at $\nu = 0$ needed to be introduced in a singly-subtracted dispersion relation[11],[14].

Again, following Block and Cahn[11], we now introduce three types of odderon laboratory amplitudes for forward scattering, $f_-^{(j)}$, where $j = 0, 1$, or 2 . Introducing the laboratory energy $\nu = \sqrt{p^2 + m^2}$, where m is the proton mass, they are:

$$f_-^{(0)} = -\frac{1}{4\pi}\epsilon^{(0)}\nu, \quad (4)$$

$$f_-^{(1)} = -\frac{1}{4\pi}\epsilon^{(1)}\nu \left[\ln(s/s_0) - i\frac{\pi}{2} \right], \quad (5)$$

$$f_-^{(2)} = -\frac{1}{4\pi}\epsilon^{(2)}\nu \left[\ln(s/s_0) - i\frac{\pi}{2} \right]^2, \quad (6)$$

where the $\epsilon^{(j)}$ $j = 0, 1, 2$ are all real coefficients. These amplitudes, called odderon 0, odderon 1 and odderon 2, respectively, are manifestly odd, since they are all proportional to ν times an even amplitude. Clearly, the laboratory energy ν is odd under crossing ($\nu \rightarrow -\nu$), whereas terms like $[\ln(s/s_0) - i\frac{\pi}{2}]$ are even under crossing, so that their overall product, $f_-^{(j)}$, is crossing-odd. It can be shown that odderon 2 is the ‘maximal’ odderon allowed by unitarity and the Froissart bound (see Eqns. (4.114) and (4.115) of Ref. [11]). We will

combine these odderons individually with the conventional odd amplitude of Eq. (3) to form a new total odd amplitude. Since it is pure real, the amplitude $f_-^{(0)}$ only causes a small splitting in the ρ -values at high energy; the amplitude $f_-^{(1)}$ has a constant imaginary part, so that it leads to a constant non-zero $\Delta\sigma$, while its real part causes the ρ -values to split apart at high energy; finally, the amplitude $f_-^{(2)}$ has an imaginary part that causes $\Delta\sigma \rightarrow \ln(s/s_0)$ as $s \rightarrow \infty$, along with a real part that causes a substantial splitting of the ρ -values at high energies. We have chosen these amplitudes to be identical to those that were used by Block and Cahn[11] in their work, so that at the end of our analysis we can make a direct comparison of our odderon coefficients $\epsilon^{(j)}$ with theirs. We comment that that these real analytic forward scattering amplitudes, Eq. (2)–Eq. (6), can also be derived as solutions to derivative dispersion relations[2].

Using the optical theorem and our laboratory forward scattering amplitude normalization, we write

$$\sigma_{\text{even}} = \frac{4\pi}{p} \text{Im} f_+ \quad (7)$$

$$\sigma_{\text{odd}} = \frac{4\pi}{p} \text{Im} f_-, \quad (8)$$

the even and odd (under crossing) cross sections due to the even and odd forward laboratory amplitudes f_+ and f_- , respectively. These cross section sums and differences

$$\sigma(pp) \equiv \sigma_{\text{even}} + \sigma_{\text{odd}}, \quad (9)$$

$$\sigma(\bar{p}p) \equiv \sigma_{\text{even}} - \sigma_{\text{odd}}, \quad (10)$$

give rise to the pp and the $\bar{p}p$ cross sections, respectively.

We remind the reader that the optical theorem states that the cross section contributions of the amplitudes of Eq. (4), Eq. (5) and Eq. (6) are obtained by multiplying $\text{Im} f_-^{(j)}$ by $4\pi/p$. Thus, we see that what is needed to combine an odderon amplitude with the normal amplitude is the term $\frac{4\pi}{p} f_-^{(j)}$. Using the optical theorem and analyticity in the high energy limit where $p = \nu$ —after noting that $\frac{4\pi}{p} f_-^{(j)}$ can be replaced by $\frac{4\pi}{\nu} f_-^{(j)}$ —we obtain the total cross sections $\sigma_{(j)}^\pm$ and $\rho_{(j)}^\pm$, the ratios of the real to the imaginary portion of the forward scattering amplitude, for $j = 0, 1, 2$, as

$$\sigma_{(0)}^\pm = A + \beta \left[\ln^2 s/s_0 - \frac{\pi^2}{4} \right] + c \sin(\pi\mu/2) s^{\mu-1} \pm D \cos(\pi\alpha/2) s^{\alpha-1}, \quad (11)$$

$$\rho_{(0)}^\pm = \frac{1}{\sigma_{(0)}^\pm} \left\{ \beta \pi \ln s/s_0 - c \cos(\pi\mu/2) s^{\mu-1} + \frac{4\pi}{\nu} f_+(0) \pm D \sin(\pi\alpha/2) s^{\alpha-1} \pm \epsilon^{(0)} \right\}, \quad (12)$$

or

$$\sigma_{(1)}^\pm = A + \beta \left[\ln^2 s/s_0 - \frac{\pi^2}{4} \right] + c \sin(\pi\mu/2) s^{\mu-1} \pm D \cos(\pi\alpha/2) s^{\alpha-1} \mp \epsilon^{(1)} \frac{\pi}{2}, \quad (13)$$

$$\rho_{(1)}^\pm = \frac{1}{\sigma_{(1)}^\pm} \left\{ \beta \pi \ln s/s_0 - c \cos(\pi\mu/2) s^{\mu-1} + \frac{4\pi}{\nu} f_+(0) \pm D \sin(\pi\alpha/2) s^{\alpha-1} \pm \epsilon^{(1)} \ln(s/s_0) \right\}, \quad (14)$$

or

$$\sigma_{(2)}^\pm = A + \beta \left[\ln^2 s/s_0 - \frac{\pi^2}{4} \right] + c \sin(\pi\mu/2) s^{\mu-1} \pm D \cos(\pi\alpha/2) s^{\alpha-1} \mp \epsilon^{(2)} \pi \ln(s/s_0), \quad (15)$$

$$\rho_{(2)}^\pm = \frac{1}{\sigma_{(2)}^\pm} \left\{ \beta \pi \ln s/s_0 - c \cos(\pi\mu/2) s^{\mu-1} + \frac{4\pi}{\nu} f_+(0) \pm D \sin(\pi\alpha/2) s^{\alpha-1} \right. \quad (16)$$

$$\left. \pm \epsilon^{(2)} \left(\ln^2(s/s_0) - \frac{\pi^2}{4} \right) \right\}, \quad (17)$$

where the upper sign is for pp and the lower sign is for $\bar{p}p$ scattering.

We now introduce the definitions

$$A = c_0 + \frac{\pi^2}{4}c_2 - \frac{c_1^2}{4c_2}, \quad (18)$$

$$s_0 = 2m^2 e^{-c_1/(2c_2)}, \quad (19)$$

$$\beta = c_2, \quad (20)$$

$$c = \frac{(2m^2)^{1-\mu}}{\sin(\pi\mu/2)} \beta_{\mathcal{P}'}, \quad (21)$$

$$D = \frac{(2m^2)^{1-\alpha}}{\cos(\pi\alpha/2)} \delta. \quad (22)$$

After some algebraic manipulations, the cross sections $\sigma_{(j)}^\pm$ and the ρ -values $\rho_{(j)}^\pm$, along with the cross section derivatives $\frac{d\sigma_{(j)}^\pm}{d(\nu/m)}$, can now be written as

$$\sigma_{(0)}^\pm(\nu) = c_0 + c_1 \ln\left(\frac{\nu}{m}\right) + c_2 \ln^2\left(\frac{\nu}{m}\right) + \beta_{\mathcal{P}'} \left(\frac{\nu}{m}\right)^{\mu-1} \pm \delta \left(\frac{\nu}{m}\right)^{\alpha-1}, \quad (23)$$

$$\rho_{(0)}^\pm(\nu) = \frac{1}{\sigma_{(0)}^\pm} \left\{ \frac{\pi}{2} c_1 + c_2 \pi \ln\left(\frac{\nu}{m}\right) - \beta_{\mathcal{P}'} \cot\left(\frac{\pi\mu}{2}\right) \left(\frac{\nu}{m}\right)^{\mu-1} + \frac{4\pi}{\nu} f_+(0) \right. \\ \left. \pm \delta \tan\left(\frac{\pi\alpha}{2}\right) \left(\frac{\nu}{m}\right)^{\alpha-1} \pm \epsilon^{(0)} \right\}, \quad (24)$$

$$\frac{d\sigma_{(0)}^\pm(\nu)}{d(\nu/m)} = c_1 \left\{ \frac{1}{(\nu/m)} \right\} + c_2 \left\{ \frac{2 \ln(\nu/m)}{(\nu/m)} \right\} + \beta_{\mathcal{P}'} \{(\mu-1)(\nu/m)^{\mu-2}\} \pm \delta \{(\alpha-1)(\nu/m)^{\alpha-2}\} \quad (25)$$

or

$$\sigma_{(1)}^\pm(\nu) = c_0 + c_1 \ln\left(\frac{\nu}{m}\right) + c_2 \ln^2\left(\frac{\nu}{m}\right) + \beta_{\mathcal{P}'} \left(\frac{\nu}{m}\right)^{\mu-1} \pm \delta \left(\frac{\nu}{m}\right)^{\alpha-1} \mp \epsilon^{(1)} \frac{\pi}{2}, \quad (26)$$

$$\rho_{(1)}^\pm(\nu) = \frac{1}{\sigma_{(1)}^\pm} \left\{ \frac{\pi}{2} c_1 + c_2 \pi \ln\left(\frac{\nu}{m}\right) - \beta_{\mathcal{P}'} \cot\left(\frac{\pi\mu}{2}\right) \left(\frac{\nu}{m}\right)^{\mu-1} + \frac{4\pi}{\nu} f_+(0) \right. \\ \left. \pm \delta \tan\left(\frac{\pi\alpha}{2}\right) \left(\frac{\nu}{m}\right)^{\alpha-1} \pm \epsilon^{(1)} \ln(s/s_0) \right\}, \quad (27)$$

$$\frac{d\sigma_{(1)}^\pm(\nu)}{d(\nu/m)} = c_1 \left\{ \frac{1}{(\nu/m)} \right\} + c_2 \left\{ \frac{2 \ln(\nu/m)}{(\nu/m)} \right\} + \beta_{\mathcal{P}'} \{(\mu-1)(\nu/m)^{\mu-2}\} \pm \delta \{(\alpha-1)(\nu/m)^{\alpha-2}\} \quad (28)$$

or

$$\sigma_{(2)}^\pm(\nu) = c_0 + c_1 \ln\left(\frac{\nu}{m}\right) + c_2 \ln^2\left(\frac{\nu}{m}\right) + \beta_{\mathcal{P}'} \left(\frac{\nu}{m}\right)^{\mu-1} \pm \delta \left(\frac{\nu}{m}\right)^{\alpha-1} \mp \epsilon^{(2)} \pi \ln(s/s_0), \quad (29)$$

$$\rho_{(2)}^\pm(\nu) = \frac{1}{\sigma_{(2)}^\pm} \left\{ \frac{\pi}{2} c_1 + c_2 \pi \ln\left(\frac{\nu}{m}\right) - \beta_{\mathcal{P}'} \cot\left(\frac{\pi\mu}{2}\right) \left(\frac{\nu}{m}\right)^{\mu-1} + \frac{4\pi}{\nu} f_+(0) \right. \\ \left. \pm \delta \tan\left(\frac{\pi\alpha}{2}\right) \left(\frac{\nu}{m}\right)^{\alpha-1} \pm \epsilon^{(2)} \left(\ln^2(s/s_0) - \frac{\pi^2}{4} \right) \right\}, \quad (30)$$

$$\frac{d\sigma_{(2)}^\pm(\nu)}{d(\nu/m)} = c_1 \left\{ \frac{1}{(\nu/m)} \right\} + c_2 \left\{ \frac{2 \ln(\nu/m)}{(\nu/m)} \right\} + \beta_{\mathcal{P}'} \{(\mu-1)(\nu/m)^{\mu-2}\} \mp \epsilon^{(2)} \left\{ \frac{\pi}{(\nu/m)} \right\} \\ \pm \delta \{(\alpha-1)(\nu/m)^{\alpha-2}\}, \quad (31)$$

in the high energy limit where $s \rightarrow 2m\nu$, where the upper sign is for pp and the lower sign is for $\bar{p}p$ scattering. Units of σ in mb, and ν and m in GeV, where m is the proton mass, will be used. We will use $\mu = 0.5$, the value¹ used by Block and Halzen[10], which is appropriate for a Regge-descending trajectory. The new even

¹We use the value $\mu = 0.5$ in order to be able to directly compare our results, using the same data set, the same high energy parametrization and the same constraints, with an analysis[10] which used $\epsilon^{(j)} = 0$, $j = 0, 1, 2$, i.e., had no odderon amplitudes in its parametrization.

coefficients $c_0, c_1, c_2, \beta_{\mathcal{P}'}$ and the odd coefficient δ , along with the exponents μ and α , are all real. These transformations linearize Eq. (23), Eq. (26) and Eq. (29) in the parameters $c_0, c_1, c_2, \beta_{\mathcal{P}'}$ and δ , convenient for a χ^2 fit to the experimental total cross sections and ρ -values.

We will use new analyticity constraints[13] in the fitting of the $\bar{p}p$ and pp data that anchor the theoretical cross sections and their derivatives of our high energy parametrization with *experimental* cross sections and their derivatives at a transition energy ν_0 which is just above the resonance region. Let σ^+ and σ^- be the total cross sections for pp and $\bar{p}p$ scattering. It is convenient to define 4 *experimental* quantities evaluated at the transition energy ν_0 . The transition energy ν_0 is a low energy after which resonance behavior finishes. Following Block and Halzen[10], we will choose $\nu_0 = 7.59$ GeV (corresponding to $\sqrt{s_0} = 4$ GeV).

We now introduce 4 new well-determined experimental quantities, 2 crossing even quantities σ_{av} and m_{av} and 2 crossing-odd quantities $\Delta\sigma$ and Δm ,

$$\begin{aligned}\sigma_{\text{av}} &\equiv \frac{\sigma^+(\nu_0/m) + \sigma^-(\nu_0/m)}{2}, \\ \Delta\sigma &\equiv \frac{\sigma^+(\nu_0/m) - \sigma^-(\nu_0/m)}{2}, \\ m_{\text{av}} &\equiv \frac{1}{2} \left(\frac{d\sigma^+}{d(\nu/m)} + \frac{d\sigma^-}{d(\nu/m)} \right)_{\nu=\nu_0}, \\ \Delta m &\equiv \frac{1}{2} \left(\frac{d\sigma^+}{d(\nu/m)} - \frac{d\sigma^-}{d(\nu/m)} \right)_{\nu=\nu_0},\end{aligned}\tag{32}$$

capitalizing on the very accurate low energy experimental pp and $\bar{p}p$ cross section data that are available.

Using σ_{av} and m_{av} , we now write the 2 crossing-even analyticity constraint equations as

$$\beta_{\mathcal{P}'} = \frac{(\nu_0/m)^{2-\mu}}{\mu-1} \left[m_{\text{av}} - c_1 \left\{ \frac{1}{(\nu_0/m)} \right\} - c_2 \left\{ \frac{2 \ln(\nu_0/m)}{(\nu_0/m)} \right\} \right],\tag{33}$$

$$c_0 = \sigma_{\text{av}} - c_1 \ln(\nu_0/m) - c_2 \ln^2(\nu_0/m) - \beta_{\mathcal{P}'} (\nu_0/m)^{\mu-1},\tag{34}$$

reiterating that Eq. (33) and Eq. (34) utilize the *experimental* even cross section σ_{av} and its slope m_{av} evaluated at the transition energy ν_0 , where we join on to the asymptotic fit.

The situation is a little more complicated for the crossing-odd constraints. For odderon 0, we have

$$\alpha = 1 + \frac{\Delta m}{\Delta\sigma} \times \frac{\nu_0}{m}, \quad j = 0,\tag{35}$$

$$\delta = \Delta\sigma \times \left(\frac{\nu_0}{m} \right)^{1-\alpha},\tag{36}$$

whereas for odderon 1, we find

$$\alpha = 1 + \frac{\Delta m}{\Delta\sigma - \epsilon^{(1)}(\frac{\pi}{2})} \times \frac{\nu_0}{m}, \quad j = 1,\tag{37}$$

$$\delta = \Delta\sigma \times \left(\frac{\nu_0}{m} \right)^{1-\alpha},\tag{38}$$

and for odderon 2,

$$\alpha = 1 + \frac{\Delta m - \epsilon^{(2)}\{\pi\nu_0/m\}}{\Delta\sigma - \epsilon^{(2)}\{\pi \ln(2m\nu_0/s_0)\}} \times \frac{\nu_0}{m}, \quad j = 2,\tag{39}$$

$$\delta = \Delta\sigma \times \left(\frac{\nu_0}{m} \right)^{1-\alpha},\tag{40}$$

where $s_0 = 22.9$ GeV², which is the approximate value of s_0 found from the fit parameters of Table 2, using Eq. (19). Again, the crossing-odd constraints $\Delta\sigma$ and Δm are fixed by the *experimental* pp and $\bar{p}p$ cross sections and their derivatives at the transition energy ν_0 .

Utilizing the rich amount of accurate low energy data at the transition energy ν_0 , we have now constrained our high energy fit at $\nu_0 = 7.59$ GeV[10]. For safety, the data fitting is started at an energy $\nu_{\text{min}} = 18.25$ GeV (corresponding to $\sqrt{s_{\text{min}}} = 6$ GeV), appreciably higher than the transition energy (see footnote 1).

The appropriate cross sections and slopes, taken from ref. [10], are summarized in Table 1, along with the minimum energies used in the asymptotic fits (see footnote 1). Very local fits had been made to the region about the energy ν_0 in order to evaluate the two cross sections and their two derivatives at ν_0 that were needed in the above constraint equations. We next impose the 4 constraint equations arising from analyticity[13]:

- For Odderon 0, the Equations (33), (34), (35) and (36), are used in our χ^2 fit to Equations (23) and (24).
- For Odderon 1, the Equations (33), (34), (37) and (38), are used in our χ^2 fit to Equations (26) and (27).
- For Odderon 2, the Equations (33), (34), (39) and (40) are used in our χ^2 fit to Equations (29) and (30).

We stress that the odd amplitude parameters α and δ and hence the odd amplitude itself is *completely determined* by the experimental values Δm and $\Delta\sigma$ at the transition energy ν_0 and the value of $\epsilon^{(j)}$, $j = 0, 1, 2$. Further, the even amplitude parameters c_0 and β_p are now determined by c_1 and c_2 , along with the experimental values of σ_{av} and m_{av} at the transition energy ν_0 . In particular, we only fit the 4 parameters c_1 , c_2 , $f_+(0)$ and $\epsilon^{(j)}$, $j = 0, 1, 2$. Since the subtraction constant $f_+(0)$ enters only into the ρ -value determinations, of the original 8 free parameters that were needed to be fit for a $\ln^2 s$ energy dependence of the cross sections σ^\pm , only the 3 parameters c_1 , c_2 and $\epsilon^{(j)}$, $j = 0, 1, 2$ are now free, giving us exceedingly little freedom in this fit—it is indeed very tightly constrained, with little latitude for adjustment.

The adaptive Sieve algorithm[15] that minimizes the effect that “outliers”—points with abnormally high contributions to χ^2 —have on a fit when they contaminate a data sample that is otherwise Gaussianly distributed is described in Refs. [10] and [15]. The sieved data set that we will use for our χ^2 fit to σ_{pp} , $\sigma_{\bar{p}p}$, ρ_{pp} and $\rho_{\bar{p}p}$ for $\sqrt{s} \geq 6$ GeV is detailed in Ref. [10], where Block and Halzen found that the 25 points that were screened out had a χ^2 contribution of ≈ 980 , an average value of ≈ 39 , using the cut $\Delta\chi_{i\max}^2 = 6$. For a Gaussian distribution, about 3 points with $\Delta\chi_i^2 > 6$ are expected, giving a total χ^2 contribution of slightly more than 18 and *not* 980. The effect of the “Sieve” algorithm in ridding the data sample of outliers is major.

Table 2 summarizes the results of our 3 simultaneous fits to the available accelerator data, using the sieved data set of ref. [10] which was obtained after using the “Sieve” algorithm on the Particle Data Group[16] compendium for σ_{pp} , $\sigma_{\bar{p}p}$, ρ_{pp} and $\rho_{\bar{p}p}$, using a minimum fitting energy $\sqrt{s_{\min}} = 6$ GeV and imposing the cut $\Delta\chi_{i\max}^2 = 6$. The fits were made using 4 constraint equations with a transition energy $\sqrt{s_0} = 4$ GeV, for odderons 0, 1 and 2. Very satisfactory probabilities (~ 0.2) for 183 degrees of freedom were found for all 3 odderon choices.

We summarize our results below:

- Odderon 0: Figure 1 shows the individual fitted cross sections (in mb) for pp and $\bar{p}p$ for odderon 0 in Table 2, plotted against the c.m. (center-of-mass) energy \sqrt{s} , in GeV. The data shown are the sieved data which have energies $\sqrt{s} \geq 6$ GeV. The fits to the data sample with $\Delta\chi_{i\max}^2 = 6$, corresponding to the dotted curve for $\bar{p}p$ and the solid curve for pp , are excellent, yielding a total renormalized $\chi^2 = 201.2$, for 183 degrees of freedom, corresponding to a fit probability of ~ 0.2 . Figure 2 shows the simultaneously fitted ρ -values for pp and $\bar{p}p$ for odderon 0 from Table 2, plotted against the c.m. energy \sqrt{s} , in GeV. The data shown are the sieved data with $\sqrt{s} \geq 6$ GeV. The solid curve for $\bar{p}p$ and the dotted curve for pp fit the data reasonably well. It should be noted from Table 2 that the magnitude of odderon 0 is $\epsilon^{(0)} = -0.034 \pm 0.073$ mb, a very small coefficient. Indeed, it is compatible with zero.
- Odderon 1: Figure 3 shows the individual fitted cross sections (in mb) for pp and $\bar{p}p$ for odderon 1 in Table 2, plotted against the c.m. energy \sqrt{s} , in GeV. The data shown are the sieved data which have energies $\sqrt{s} \geq 6$ GeV. The fits to the data sample with $\Delta\chi_{i\max}^2 = 6$, corresponding to the dotted curve for $\bar{p}p$ and the solid curve for pp , are excellent, yielding a total renormalized $\chi^2 = 200.9$, for 183 degrees of freedom, corresponding to a fit probability of ~ 0.2 . Figure 4 shows the simultaneously fitted ρ -values for pp and $\bar{p}p$ for odderon 1 from Table 2, plotted against the c.m. energy \sqrt{s} , in GeV.

The data shown are the sieved data with $\sqrt{s} \geq 6$ GeV. The solid curve for $\bar{p}p$ and the dotted curve for pp fit the data reasonably well. It should be noted from Table 2 that the magnitude of odderon 1 is $\epsilon^{(1)} = -0.0051 \pm 0.0077$ mb, a very tiny coefficient which is again compatible with zero.

- Odderon 2: Figure 5 shows the individual fitted cross sections (in mb) for pp and $\bar{p}p$ for odderon 2 in Table 2, plotted against the c.m. energy \sqrt{s} , in GeV. The data shown are the sieved data which have energies $\sqrt{s} \geq 6$ GeV. The fits to the data sample with $\Delta\chi_{i\max}^2 = 6$, corresponding to the dotted curve for $\bar{p}p$ and the solid curve for pp , are excellent, yielding a total renormalized $\chi^2 = 196.1$, for 183 degrees of freedom, corresponding to a fit probability of ~ 0.2 . Figure 6 shows the simultaneously fitted ρ -values for pp and $\bar{p}p$ for odderon 2 from Table 2, plotted against the c.m. energy \sqrt{s} , in GeV. The data shown are the sieved data with $\sqrt{s} \geq 6$ GeV. The solid curve for $\bar{p}p$ and the dotted curve for pp fit the data reasonably well. It should be noted from Table 2 that the magnitude of odderon 2 is $\epsilon^{(2)} = 0.0042 \pm 0.0019$ mb, a very tiny coefficient which is only about two standard deviations from zero.

In Table 3, we make predictions of total cross sections and ρ -values for $\bar{p}p$ and pp scattering for odderon 2 of Table 2. Only for *very* high energies above $\sqrt{s} = 14$ TeV is there any appreciable difference between $\rho_{\bar{p}p}$ and ρ_{pp} , as seen in Fig. 6. In fact, the results of all 3 fits are very close to what was found in ref. [10], where there were no odderon amplitudes, but had virtually identical $\chi^2/\text{d.f.}$

These new upper limits on odderon amplitudes are to be contrasted to the analysis made in 1985 by Block and Cahn[11], where they found $\epsilon^{(0)} = -0.25 \pm 0.13$ mb, $\epsilon^{(1)} = -0.11 \pm 0.04$ mb and $\epsilon^{(2)} = -0.04 \pm 0.02$ mb, which were about two standard deviations from zero, but with errors of almost 2 to 10 times larger than the limits found in this note. Our marked increase in present accuracy is attributable to the use of the 4 analyticity constraints[13] employed in the present analysis, as well as to the use of the improved sieved data set[10, 15], which also has higher energy points than were available in 1985.

In conclusion, the magnitude of all three odderon amplitudes, $\epsilon^{(0)} = -0.034 \pm 0.073$ mb, $\epsilon^{(1)} = -0.00051 \pm 0.0077$ mb and $\epsilon^{(2)} = 0.0042 \pm 0.0019$ mb, in comparison to all of the other amplitudes found in the fit—typically of the order of 1.5 to 40 mb—are very tiny. Indeed, all 3 are compatible with zero and we now can set new upper limits a factor of 2 better for $\epsilon^{(0)}$, a factor of 5 better for $\epsilon^{(1)}$ and a factor of 10 better for the maximum odderon $\epsilon^{(2)}$. An accurate measurement of the ρ -value at the LHC, where Block and Halzen[10] predict $\rho_{pp} = 0.132 \pm 0.001$ when odderon amplitudes are zero and our prediction from from Table 3 is $\rho_{pp} = 0.141 \pm 0.005$, would really constrain the maximal odderon amplitude $\epsilon^{(2)}$.

Acknowledgments

One of us (MMB) would like to acknowledge the hospitality of the Aspen Center for Physics, Aspen, CO, during the preparation of this work. One of us (KK) was supported in part by the Department of Energy contract DE-FG02-91Er40688 Task A.

References

- [1] L. Lukaszuk and B. Nicolescu, *Lett. Nuovo Cimento* **8**, 405 (1973).
- [2] K. Kang and B. Nicolescu, *Phys. Rev. D* **11**, 2461 (1975). This was the first group to apply derivative dispersion relations to the derivation of real analytic amplitudes.
- [3] D. Joynson et al, *Nuovo Cimento* **A30**, 345 (1975).
- [4] M. M. Block and K. Kang, *Int. J. Mod. Phys. A* **20**, 2781 (2005).
- [5] J. R. Cudell *et al.*, *Phys. Rev. D* **65**, 074024 (2002); (COMPETE Collaboration) *Phys. Rev. Lett.* **89**, 201801 (2002).
- [6] K. Igi and M. Ishida, *Phys. Rev. D* **66**, 034023 (2002).
- [7] K. Igi and M. Ishida, *Phys. Lett.* **B622**, 286 (2005).
- [8] K. Kang and H. Nastase, *Phys. Rev. D* **72**, 106003 (2005); *Phys. Lett. B* **624**, 125 (2005).
- [9] M. M. Block and F. Halzen, **hep-ph0405174** (2004); *Phys. Rev. D* **70**, 091901 (2004).
- [10] M. M. Block and F. Halzen, *Phys. Rev D* **72**, 036006 (2005).
- [11] M. M. Block and R. N. Cahn, *Rev. Mod. Phys.* **57**, 563 (1985).
- [12] M. M. Block, *Phys. Rev. D* **65**, 116005 (2002).
- [13] M. M. Block, **hep-ph0601210** (2006).
- [14] For the reaction $\gamma + p \rightarrow \gamma + p$, it is fixed as the Thompson scattering limit $f_+(0) = -\alpha/m = -3.03 \mu\text{b GeV}$ [see M. Damashek and F. J. Gilman, *Phys. Rev. D* **1**, 1319 (1970)].
- [15] M. M. Block, **physics/0506010** (2005); *Nucl. Inst. and Meth. A.* **556**, 308 (2006).
- [16] Particle Data Group, K. Hagiwara et al., *Phys. Rev. D* **66**, 010001 (2002).

| | |
|--|---------|
| ν_0 , lab transition energy (GeV) | 7.59 |
| $\rightarrow \sqrt{s_0}$, c.m. transition energy (GeV) | 4 |
| $\sigma_+(\nu_0)$ (mb) | 40.18 |
| $\sigma_-(\nu_0)$ (mb) | 56.99 |
| $\left(\frac{d\sigma_+}{d(\nu/m)}\right)_{\nu=\nu_0}$ (mb) | -0.2305 |
| $\left(\frac{d\sigma_-}{d(\nu/m)}\right)_{\nu=\nu_0}$ (mb) | -1.446 |
| Minimum fitting energy | |
| ν_{\min} , lab minimum energy (GeV) | 18.25 |
| $\rightarrow \sqrt{s_{\min}}$, c.m. minimum energy (GeV) | 6.0 |

m is the proton mass and ν is the laboratory proton energy

Table 1: The transition energy parameters and minimum fitting energy used for constraining pp and $\bar{p}p$ scattering. Taken from ref. [10].

| Parameters | odderon 0 | odderon 1 | odderon 2 |
|--|---------------------|----------------------|---------------------|
| | Even Amplitude | | |
| c_0 (mb) | 37.38 | 37.24 | 37.09 |
| c_1 (mb) | -1.460 ± 0.065 | -1.415 ± 0.073 | -1.370 ± 0.0074 |
| c_2 (mb) | 0.2833 ± 0.0060 | 0.2798 ± 0.0064 | 0.2771 ± 0.0064 |
| $\beta_{\mathcal{P}'}$ (mb) | 37.02 | 37.20 | 37.39 |
| μ | 0.5 | 0.5 | 0.5 |
| $f_+(0)$ (mb GeV) | -0.075 ± 0.75 | -0.050 ± 0.59 | $-.073 \pm 0.58$ |
| | Odd Amplitude | | |
| δ (mb) | -28.56 | -28.53 | -28.49 |
| α | 0.415 | 0.416 | 0.416 |
| $\epsilon^{(j)}$ (mb), $j = 0, 1, 2$ | -0.034 ± 0.073 | -0.0051 ± 0.0077 | 0.0042 ± 0.0019 |
| χ_{\min}^2 | 181.3 | 181.1 | 176.7 |
| $\mathcal{R} \times \chi_{\min}^2$ | 201.2 | 200.9 | 196.1 |
| degrees of freedom (d.f.) | 183 | 183 | 183 |
| $\mathcal{R} \times \chi_{\min}^2/\text{d.f.}$ | 1.099 | 1.098 | 1.071 |

Table 2: The fitted results for a 4-parameter χ^2 fit using odderons 0, 1 and 2, with $\sigma \sim \ln^2 s$, to the total cross sections and ρ -values for pp and $\bar{p}p$ scattering. The renormalized χ_{\min}^2 per degree of freedom, taking into account the effects of the $\Delta\chi_{i\max}^2 = 6$ cut, is given in the row labeled $\mathcal{R} \times \chi_{\min}^2/\text{d.f.}$ The errors in the fitted parameters have been multiplied by the appropriate r_{χ^2} . For details on the renormalization of the errors by r_{χ^2} and the renormalization of χ_{\min}^2 by \mathcal{R} , see ref. [15].

| \sqrt{s} , in GeV | $\sigma_{\bar{p}p}$, in mb | $\rho_{\bar{p}p}$ | σ_{pp} , in mb | ρ_{pp} |
|---------------------|-----------------------------|-------------------|-----------------------|-------------------|
| 300 | 55.14 ± 0.20 | 0.125 ± 0.003 | 54.82 ± 0.20 | 0.134 ± 0.003 |
| 540 | 60.89 ± 0.29 | 0.129 ± 0.004 | 60.59 ± 0.29 | 0.141 ± 0.003 |
| 1,800 | 75.19 ± 0.50 | 0.130 ± 0.001 | 74.87 ± 0.52 | 0.146 ± 0.004 |
| 14,000 | 107.1 ± 1.1 | 0.121 ± 0.005 | 106.6 ± 1.1 | 0.141 ± 0.005 |
| 50,000 | 131.55 ± 1.5 | 0.112 ± 0.006 | 131.1 ± 1.6 | 0.134 ± 0.005 |
| 100,000 | 146.39 ± 1.8 | 0.108 ± 0.006 | 145.9 ± 1.9 | 0.131 ± 0.005 |

Table 3: Predictions of high energy $\bar{p}p$ and pp total cross sections and ρ -values for odderon 2, from Table 2.

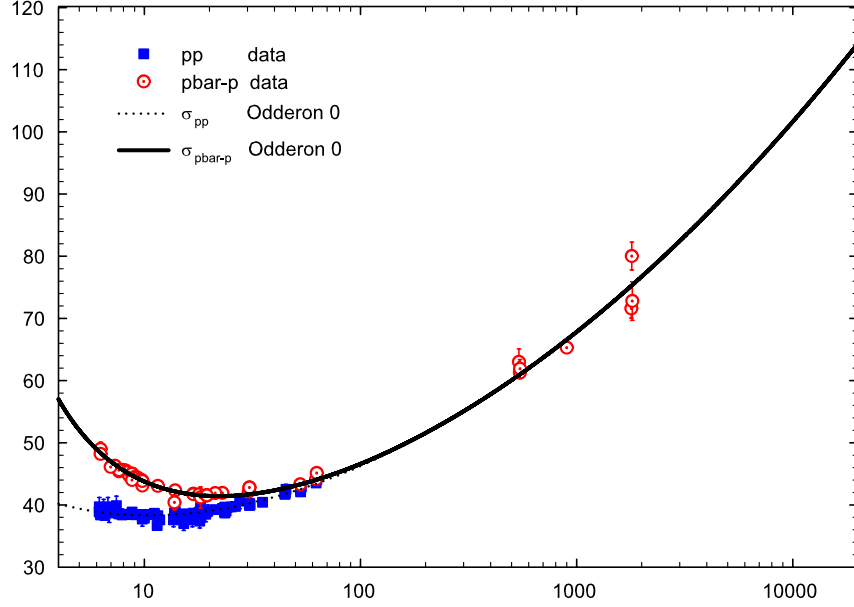


Figure 1: Odderon 0: The fitted total cross sections $\sigma_{\bar{p}p}$ and σ_{pp} in mb, vs. \sqrt{s} , in GeV, using the 4 constraints of Equations (33), (34), (35) and (36), for odderon 0 of Eq. (4). The circles are the sieved data for $\bar{p}p$ scattering and the squares are the sieved data for pp scattering for $\sqrt{s} \geq 6$ GeV. The solid curve ($\bar{p}p$) and the dotted curve (pp) are χ^2 cross section fits, corresponding to a simultaneous fit to cross sections and ρ -values (Table 2, of odderon 0) of Eq. (23) and Eq. (24).

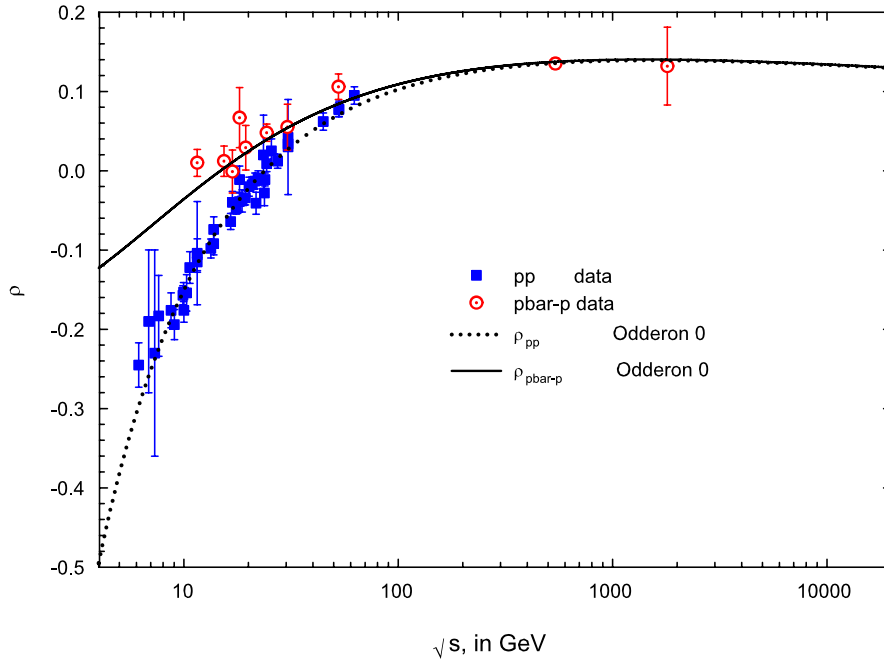


Figure 2: Odderon 0: The fitted ρ -values, $\rho_{\bar{p}p}$ and ρ_{pp} , vs. \sqrt{s} , in GeV, using the 4 constraints of Equations (33), (34), (35) and (36), for odderon 0 of Eq. (4). The circles are the sieved data for $\bar{p}p$ scattering and the squares are the sieved data for pp scattering for $\sqrt{s} \geq 6$ GeV. The solid curve ($\bar{p}p$) and the dotted curve (pp) are χ^2 cross section fits, corresponding to a simultaneous fit to cross sections and ρ -values (Table 2, of odderon 0) of Eq. (23) and Eq. (24).

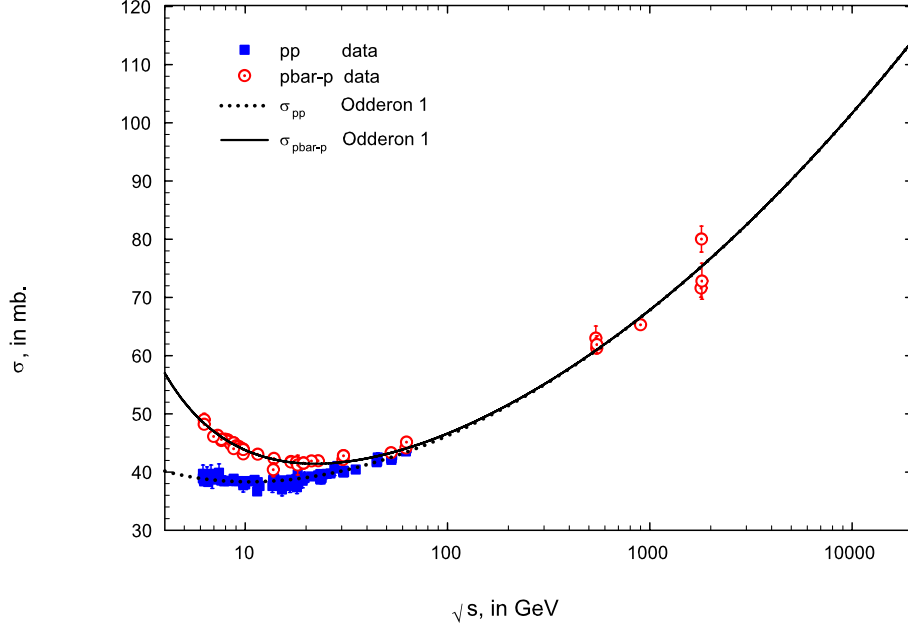


Figure 3: Odderon 1: The fitted total cross sections $\sigma_{\bar{p}p}$ and σ_{pp} in mb, vs. \sqrt{s} , in GeV, using the 4 constraints of Equations (33), (34), (37) and (38), for odderon 1 of Eq. (5). The circles are the sieved data for $\bar{p}p$ scattering and the squares are the sieved data for pp scattering for $\sqrt{s} \geq 6$ GeV. The solid curve ($\bar{p}p$) and the dotted curve (pp) are χ^2 cross section fits, corresponding to a simultaneous fit to cross sections and ρ -values (Table 2, of odderon 1) of Eq. (26) and Eq. (27).

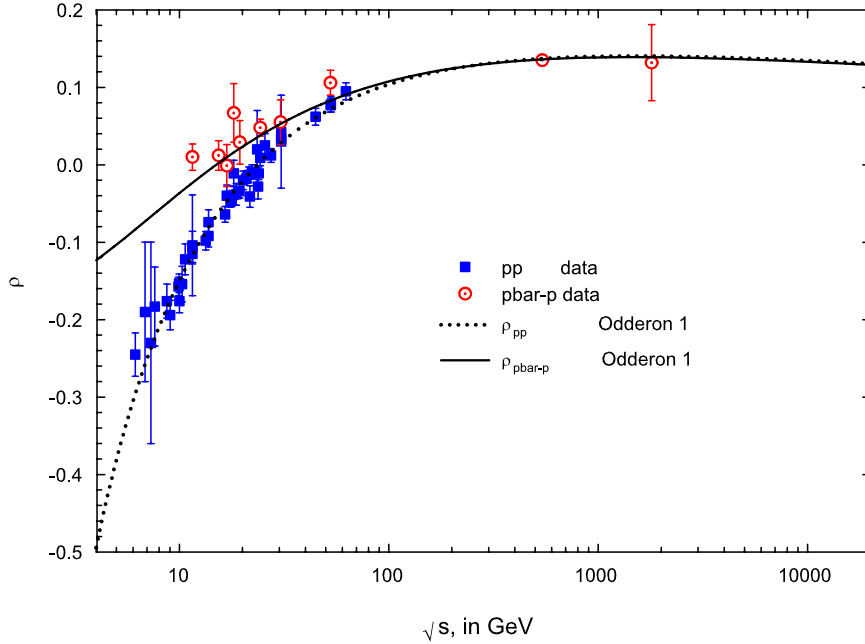


Figure 4: Odderon 1: The fitted ρ -values, $\rho_{\bar{p}p}$ and ρ_{pp} , vs. \sqrt{s} , in GeV, using the 4 constraints of Equations (33), (34), (37) and (38), for odderon 1 of Eq. (5). The circles are the sieved data for $\bar{p}p$ scattering and the squares are the sieved data for pp scattering for $\sqrt{s} \geq 6$ GeV. The solid curve ($\bar{p}p$) and the dotted curve (pp) are χ^2 cross section fits, corresponding to a simultaneous fit to cross sections and ρ -values (Table 2, of odderon 1) of Eq. (26) and Eq. (27).

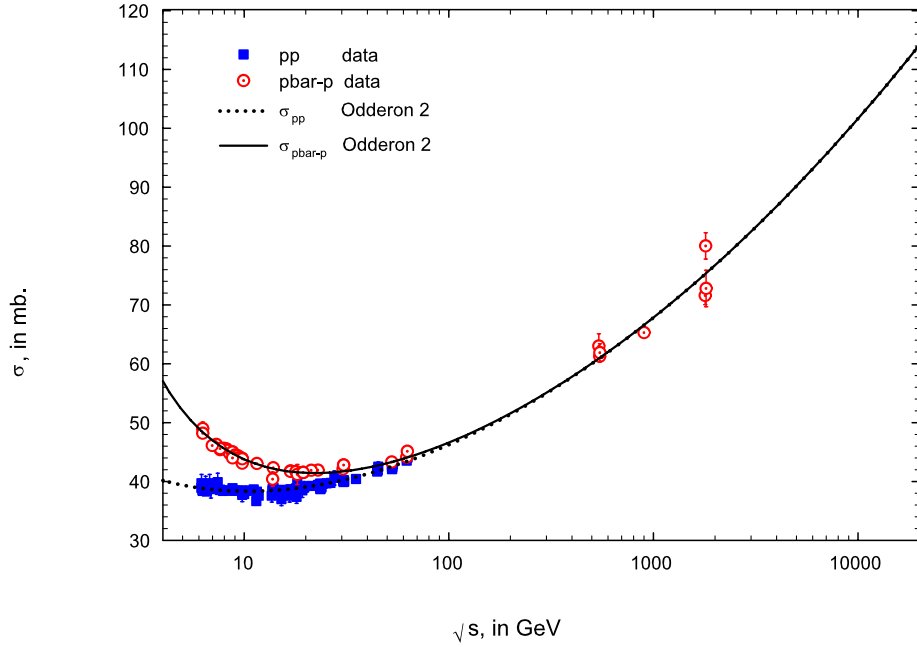


Figure 5: Odderon 2: The fitted total cross sections $\sigma_{\bar{p}p}$ and σ_{pp} in mb, vs. \sqrt{s} , in GeV, using the 4 constraints of Equations (33), (34), (39) and (40), for odderon 2 of Eq. (6). The circles are the sieved data for $\bar{p}p$ scattering and the squares are the sieved data for pp scattering for $\sqrt{s} \geq 6$ GeV. The solid curve ($\bar{p}p$) and the dotted curve (pp) are χ^2 cross section fits, corresponding to a simultaneous fit to cross sections and ρ -values (Table 2, of odderon 2) of Eq. (29) and Eq. (30).

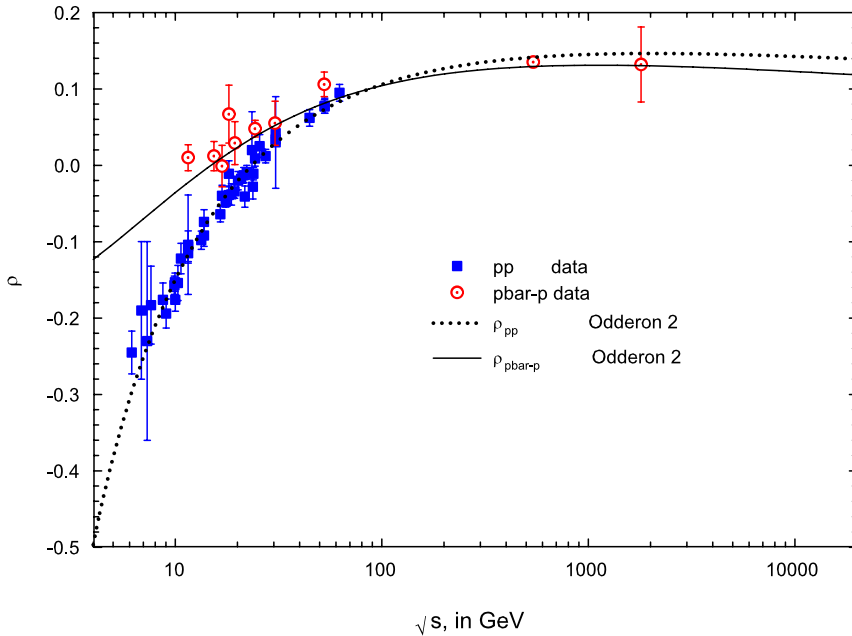


Figure 6: Odderon 2: The fitted ρ -values, $\rho_{\bar{p}p}$ and ρ_{pp} , vs. \sqrt{s} , in GeV, using the 4 constraints of Equations (33), (34), (39) and (40), for odderon 2 of Eq. (6). The circles are the sieved data for $\bar{p}p$ scattering and the squares are the sieved data for pp scattering for $\sqrt{s} \geq 6$ GeV. The solid curve ($\bar{p}p$) and the dotted curve (pp) are χ^2 cross section fits, corresponding to a simultaneous fit to cross sections and ρ -values (Table 2, of odderon 2) of Eq. (29) and Eq. (30).